Research Article | Vol. 9, No. 11 / 1 November 2019 / Optical Materials Express 4464
Optical Materials EXPRESS

# Mid-infrared spectroscopic characterization of $Pr^{3+}$:$Lu_2O_3$

**Alessandra Toncelli,[1,*] Jihua Xu,[1] Alessandro Tredicucci,[1,2] Alexander M. Heuer,[3,4] and Christian Kränkel[5]**

[1]*Istituto Nanoscienze – CNR and Dipartimento di Fisica "Enrico Fermi", Università di Pisa, Largo B. Pontecorvo, 3, 56127 Pisa, Italy*
[2]*Laboratorio NEST Scuola Normale Superiore, Piazza San Silvestro 12, 56127 Pisa, Italy*
[3]*Institut für Laser-Physik, Universität Hamburg, 22761 Hamburg, Germany*
[4]*The Hamburg Centre for Ultrafast Imaging, Universität Hamburg, 22761 Hamburg, Germany*
[5]*The Leibniz-Institut für Kristallzüchtung (IKZ) Max-Born-Str. 2, 12489 Berlin, Germany*
[*]*alessandra.toncelli@unipi.it*

**Abstract:** We report spectroscopic characterization of $Pr^{3+}$:$Lu_2O_3$ in the MIR region from 1 to 10 μm. $Lu_2O_3$ possesses good thermo-physical properties, has relatively low phonon energies, and can be grown in good quality. Moreover, $Pr^{3+}$ ions possess several low-energy levels that in principle, can give rise to mid-infrared emission. For these reasons, we investigated this material as a potential mid-infrared emitter. From absorption measurements, we identified absorption from the first five multiplets. Moreover, low temperature measurements allowed us to extract the Stark sublevel positions of all these five multiplets and we revised the classical Dieke diagram for $Pr^{3+}$ in this compound. We also observed near- and mid-infrared emission bands under diode laser pumping. The pump power dependence of the corresponding emission intensities proved the main energy transfer mechanisms that populate the lower lying levels to be cross-relaxation processes and permitted us to discern among the various possibilities and assign the different emission bands to specific transitions. In particular, we observed for the first time MIR emission at 4.4 and 7 μm in this compound, that is, in the latter case, an emission energy equal to less than three phonons in this crystal host.



## 1. Introduction

The interest in developing new coherent sources for the mid-infrared (MIR) region is increasing for a wide range of possible scientific and technological applications. In fact, MIR is called "the fingerprint region" for the large number of roto-vibrational absorption features molecules show in this range. MIR spectroscopy can then be extremely useful, for example, in trace gas sensing, medical applications, information technology, food quality control, security controls, etc. Unfortunately, most of the coherent sources here available possess intrinsic limitations concerning output peak power, beam quality and/or need of cryogenic operation which limit their use for real life applications.

For this reason, it is important to study the spectroscopic characteristics of new potential emitting materials with specific attention to the MIR range. Rare-earth-doped crystals and fibers have long been used as laser active media in the UV, VIS, and near infrared (NIR) spectral regions, and they have the potential of generating MIR laser emission as well. Up to now, a limited number of materials have shown laser emission in this range and very few beyond 4 μm [1–4], mainly because of the competition between radiative and non-radiative processes that limit the emission efficiency of these materials at long wavelengths. The ideal material must combine excellent crystal quality, good thermo-physical parameters like thermal conductivity and chemical stability, a wide transparency region in the MIR, and low phonon energies. All these

#372402 https://doi.org/10.1364/OME.9.004464
Journal © 2019 Received 22 Jul 2019; revised 21 Sep 2019; accepted 24 Sep 2019; published 31 Oct 2019

Optical Materials EXPRESS

features are very difficult to find combined in one host crystal. Most of the previous research has been focused on fluorides, bromides and chlorides [1,3,5–8] because of their very low phonon energies, but a rule of thumb is that the lower the phonon energy, the lower the chemical stability and thermal conductivity. For this reason, most of these compounds are hygroscopic and/or are not capable to withstand the high power density required for laser emission. Moreover, the crystal growth of these materials is very complicated because of the high chemical reactivity and toxicity of some of the components or by-products. Therefore the optical quality of grown samples (especially chlorides and bromides) is often low both for the presence of scattering centers and contamination with quenching centers.

Sesquioxides are a class of crystals that possess good thermo-physical properties and can be grown in good quality [9]. Among the crystals in this class, $Lu_2O_3$ is of particular interest, not just because of its high base thermal conductivity of 12.3 $Wm^{-1}K^{-1}$, but also because its thermal conductivity is almost invariant under increasing doping concentration if doped with heavy rare-earth ions [10]. This enables higher doping concentrations while maintaining a high thermal conductivity, which has led to laser results in the near and mid-infrared spectral region [11,12] and interesting spectroscopic features [13].

Many rare earth ions possess potential emission lines in the MIR [5], and trivalent Praseodymium shows some of the longest-wavelength possible transitions [5,7] which have already shown laser action in some cases [1]. For these reasons, we present a spectroscopic investigation of Pr:$Lu_2O_3$ in the range between 1.5 µm and 10 µm in order to gain deeper insight on the spectral features of this material in the MIR.

## 2. Experimental setup

Structural characterization was performed using an energy dispersive X-ray (EDX) measurement. The sample is bombarded with a stream of high-energy electrons, which leads to the ejection of electrons from the K-shell in the sample. Upon recombination, each element emits a characteristic X-ray spectrum. Gathering enough of these X-ray photons allows for calculating the concentration of certain elements in the sample.

Room temperature transmission measurements in the MIR spectral range were performed with a Fourier-transform infrared spectrometer operating under vacuum in the range between 7000 $cm^{-1}$ and 400 $cm^{-1}$ (1.43 µm – 25 µm, Jasco FT/IR6800). Low temperature measurements were performed with an open-air Fourier-transform infrared spectrometer operating in the wavenumber range between 8000 $cm^{-1}$ and 400 $cm^{-1}$ (1.25 µm - 25 µm, Nicolet Magna 860). For low temperature measurements, the sample was placed in a liquid helium continuous flow cryostat (Oxford Instruments Optistat CF-V2).

Emission measurements were performed after excitation with a laser diode emitting a continuous wave output of 1.6 W at a wavelength of 450 nm. Laser emission was focused on the sample and its intensity was varied with neutral density filters for measurements as a function of the pump power. NIR emission was collected with an optical fiber and analyzed with a compact dispersive spectrometer (Ocean Optics, HR4000). MIR emission was collected with a parabolic mirror and sent to the Nicolet Magna 860 spectrometer that is equipped to accept external sources.

## 3. Results and discussion

### 3.1. Crystal growth and structural characterization

Due to the high melting point of $Lu_2O_3$, the crystal was grown in a rhenium crucible surrounded by zirconia felts and alumina ceramic plates for insulation [14]. The starting materials lutetium oxide (99 at. %) and praseodymium oxide (1 at. %) were mixed in the desired doping concentration, heated up to the melting temperature and then slowly cooled down. The crucible is inductively heated and the atmosphere in the chamber consisted of 95% nitrogen and 5% hydrogen. After

Optical Materials EXPRESS

solidification of the melt, a similar gas mix – but containing 300 ppm oxygen – was used in order to anneal the crystal and thus eliminate oxygen vacancy sites from the crystal lattice. More details on the growth process can be found in [14]. The sample consists of large single crystalline pieces, as confirmed by X-ray analysis. The thickness of the obtained sample is 2.3 mm at an aperture of 15 mm by 12 mm (see Fig. 1(a)).

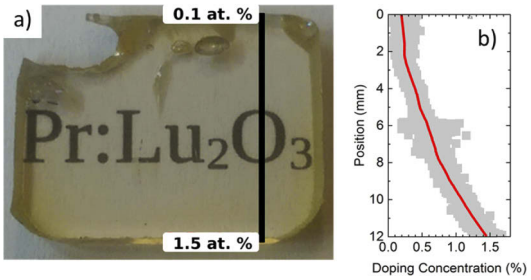


**Fig. 1.** a) Picture of the sample, b) EDX running average

The crystal structure of $Lu_2O_3$ is simple cubic in the space group Ia3 [15] and the cation density amounts to $2.858 \times 10^{-18}$ cm$^{-3}$ [16]. The melting point is 2450 °C, which can pose a challenge for the manufacturing process [17]. Table 1 summarizes the main crystal properties of this compound [11].

**Table 1. Crystal properties of sesquioxides compared to YAG[a]**

| Property | $Lu_2O_3$ | $Y_2O_3$ | YAG |
|---|---|---|---|
| Lattice symmetry | cubic | cubic | cubic |
| Density (g cm$^{-1}$) | 9.42 | 5.03 | 4.56 |
| Mohs hardness | $6\frac{1}{2}$ | $6\frac{1}{2}$ | 8 |
| Melting point (°C) | 2450 | 2430 | 1940 |
| Thermal conductivity (W m$^{-1}$K$^{-1}$) | 12.6 | 13.4 | 10.1 |
| Thermal expansion ($10^{-6}$ K$^{-1}$) | 5.8 | 8.5 | 7.7-8.2 |
| Max. phonon energy (cm$^{-1}$) | 618 | 597 | 857 |

[a]From Ref. [11]

The segregation coefficient of $Pr^{3+}$ in $Lu_2O_3$ has been determined by EDX to be 0.2. The reason for this lies in the cation radius mismatch between $Pr^{3+}$ (1.0 Å) and $Lu^{3+}$ (0.86 Å) [18], which leads to a higher probability to include lutetium instead of praseodymium during the growth process. Over the course of the growth, the praseodymium concentration in the melt steadily increases, resulting in an increase in concentration in the crystal as well. The result is the gradient shown in Fig. 1(b) where 0 mm denotes the beginning of the boule, which solidified first, and 12 mm denotes the end of the boule, which solidified last.

### 3.2. MIR absorption measurements

MIR absorption spectra were acquired in the wavenumber range between 8000 cm$^{-1}$ and 1000 cm $^{-1}$ (1.25 µm – 10 µm) at room temperature. The results are shown in Fig. 2. The crystal shows an 80% transmission level (subtracted in the absorption data) throughout this range in agreement with a 10% single-interface reflectivity calculated for a refractive index of 1.9 [11]. This measurement clearly shows that the transparency range of $Lu_2O_3$ extends throughout the MIR region up to around 8 µm.

Optical Materials EXPRESS

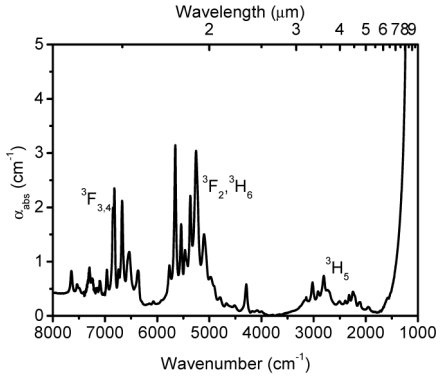


**Fig. 2.** Absorption spectrum of Pr:$Lu_2O_3$ in the near and mid infrared range

In this spectrum, different absorption bands are clearly visible. At room temperature, it is not possible to identify all the single excited multiplets because some of them are partially merged together in a single broad band constituted by many different peaks. According to the Dieke diagram [19], five excited multiplets lie in this region starting from $^3H_5$ that lies at around 2000-3300 cm$^{-1}$ (3-5 μm) and, to the best of our knowledge, has never been directly observed before in this compound. At higher energies, $^3H_6$ and $^3F_2$ are found at around 4300-5800 cm$^{-1}$ (1.7-2.3 μm), and $^3F_3$ and $^3F_4$ at around 6300-7500 cm$^{-1}$ (1.3-1.6 μm). The number of Stark level peaks in the band assigned to the multiplets $^3H_6$ and $^3F_2$ seems not to be in agreement with the expected splitting, since $^3H_6$ is expected to have up to 13 sublevels and $^3F_2$ only 5 sublevels. Low temperature absorption spectra were recorded in order to clarify this assignment.

The comparison between the absorption data recorded at 10 K and those obtained at room temperature is shown in Fig. 3 (room temperature data have been y-shifted for clarity). Since the measurements at 10 K have been performed in an open-air spectrometer, they present some atmospheric absorption noise in some regions that have been corrected, when possible.

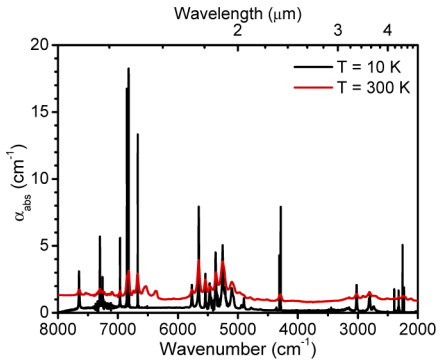


**Fig. 3.** 10 K and room temperature absorption spectra of Pr:$Lu_2O_3$ in the near and mid infrared range

As expected, the low temperature spectra consist of a fewer number of well-separated narrow lines. At 10 K only the lowest sublevel of the ground state is expected to be significantly Boltzmann populated because the first excited sublevel lies about 100 cm$^{-1}$ above [20,21]; therefore hot bands are not visible. Indeed, they are clearly visible in some of the spectral regions. For example, peaks located at around 1950 cm$^{-1}$ and 2100 cm$^{-1}$ in Fig. 4(a) and peaks located at around 6350 cm$^{-1}$ and 6550 cm$^{-1}$ in Fig. 4(d). Moreover, low temperature suppresses vibronic

Optical Materials EXPRESS

interactions and absorption lines appear much narrower than at room temperature. In the low temperature spectra, the band comprising $^3H_6$ and $^3F_2$ is clearly split in two distinct groups of peaks, the first one ranging from 5000 cm$^{-1}$ to almost 6000 cm$^{-1}$ (1.7-2 µm) with many peaks and the other at around 4300 cm$^{-1}$ (2.3 µm) with just a few peaks.

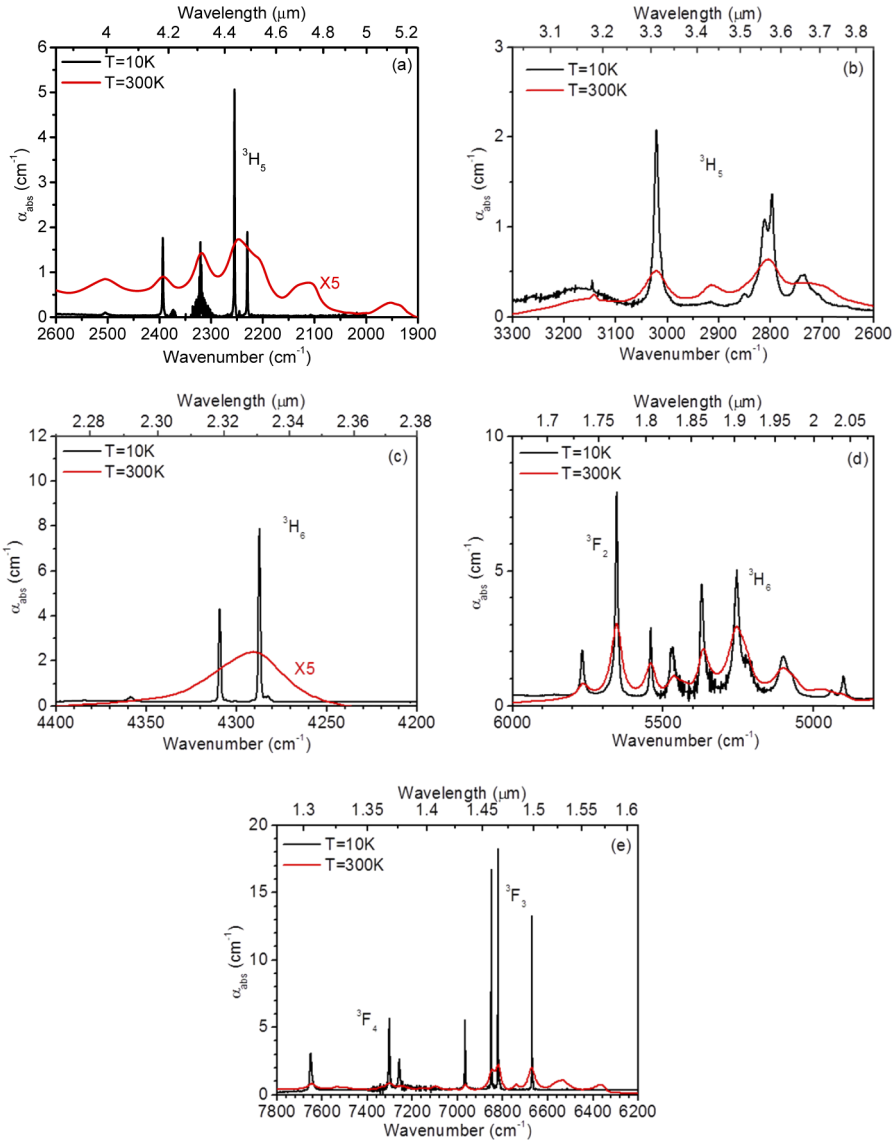


**Fig. 4.** a-e) zoom of the 10 K and room temperature absorption spectra of Pr:$Lu_2O_3$ in the near and mid infrared range

Figures 4(a)–4(e) show a zoom of the various bands. When needed, the room temperature absorption spectrum has been amplified, as indicated in the graphs.

According to these measurements, we were able to assign the energy level positions of the first five excited multiplets, as shown in Tab. 2. Starting from low energy, the region between 2200 cm $^{-1}$ and 3200 cm$^{-1}$ (3.3-4.5 µm, Fig. 4(a) and 4(b)) is assigned to $^3H_5$; it comprises 11 peaks, as expected.

Optical Materials EXPRESS

**Table 2. Energy levels of $Pr^{3+}$:$Lu_2O_3$**

| Level | Energy ($cm^{-1}$) | Level | Energy ($cm^{-1}$) | Level | Energy ($cm^{-1}$) |
|---|---|---|---|---|---|
| $^3H_5$ | 2230 | $^3H_6$ | 4282* | $^3F_2$ | 5370 |
| | 2245* | | 4287 | | 4658 |
| | 2255 | | 4301* | | 5541 |
| | 2321 | | 4306* | | 5654 |
| | 2393 | | 4309 | | 5768 |
| | 2505* | | 4359* | | |
| | 2735 | | 4381* | $^3F_3$ | 6669 |
| | 2797 | | 4779 | | 6821 |
| | 2811 | | 4900 | | 6850 |
| | 2849* | | 4940 | | 6966 |
| | 3021 | | 5071 | | |
| | | | 5100 | $^3F_4$ | 7257 |
| | | | 5154 | | 7301 |
| | | | | | 7650 |

*weak lines.

As for $^3H_6$ and $^3F_2$ according to the number of expected levels from the Dieke diagram and from [22], we assigned the highest five peaks in the region between 4200 $cm^{-1}$ and 6000 $cm^{-1}$ (1.7 µm-2.4 µm, Fig. 4(c) and 4(d)) to the $^3F_2$ multiplet, and the others to the $^3H_6$ multiplet. The number of lines perfectly matches the number of expected Stark levels, and the separation between the two multiplets occurs between two lines that are in a difference of about 120 $cm^{-1}$ from each other, which is one of the largest separations between the observed levels in the 5000 $cm^{-1}$ (2 µm) region.

The highest energy region (around 7000 $cm^{-1}$ corresponding to 1.4 µm, Fig. 4(e) comprises $^3F_3$ and $^3F_4$, and it is the most difficult to assign because the total number of high intensity peaks is much lower than expected (7 instead of 16). In addition to these peaks, a large number of weaker peaks appear mainly as sidebands of the strongest peaks. The total number of peaks in this case exceeds the theoretical number. Therefore, we retain only the strongest peaks and we assign the lower energy ones to $^3F_3$ and the higher energy ones to $^3F_4$, with some peaks missing in our assignment.

The only line that does not have the typical features of rare earth ions in crystals is a broad band from 3100 to 3300 $cm^{-1}$ (see Fig. 4(b)). This band is very broad and cannot be due to intra-multiplet absorption. Rather, it is more probably due to impurities absorption.

The result of this energy assignment together with already published results [23] for the ground state and the higher lying states is shown in Fig. 5. Possible energy transfer and nonlinear processes are also shown.

The temperature dependence of the absorption lines can give information about the origin of the lines and the interaction with the crystal phonons. We investigated the absorption spectra as a function of temperature and verified that all the absorption peaks have the typical features of rare-earth ion absorption lines; namely, the shape is Lorentzian at low temperature, the intensity decreases and the linewidth increases with temperature. In particular, the line intensity is constant at low temperature and experiences a steep temperature drop at around 100 K towards room temperature. This activation temperature is consistent with the minimum phonon energy of 90 $cm^{-1}$ measured in this crystal [24,25]. In addition, some weak lines that are not present in

Optical Materials EXPRESS

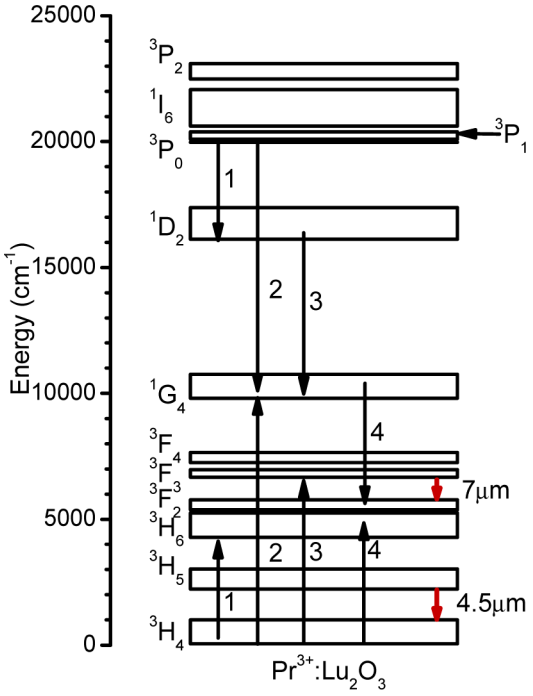


**Fig. 5.** Proposed energy level positions of Pr:$Lu_2O_3$ with some of the possible bilinear energy transfer processes that can populate low energy multiplets. Red lines show the assignment of the mid-infrared transitions observed in the next section.

the low temperature spectrum appear at higher temperature and their intensity keeps increasing up to room temperature. These can be identified as hot bands.

From the trend of the absorption spectra as a function of temperature (not shown here) we noticed that the absorption shoulder at around 3200 $cm^{-1}$ (3.1 μm) in Fig. 4(b) shows a strange temperature behavior: its intensity increases up to about 150 K, then it decreases at higher temperatures and it is hardly detectable at room temperature. This reinforces the hypothesis that it is not due to rare earth ion absorption, but has to be ascribed to unknown impurities.

### 3.3. NIR and MIR emission measurements

We also performed emission spectra under excitation with a laser diode emitting up to 1.6 W at a wavelength of 450 nm, which corresponds to absorption into the $^3P_2$ multiplet (cf. Figure 5).

From this level, a fast relaxation process is expected to populate $^3P_0$. Then, radiative decays are possible to the lower levels that in turn might emit to even lower levels. Moreover, lower lying levels can also be populated through various cross-relaxation processes. From the energy level match we can identify for example ($^3P_0$, $^3H_4$) → ($^1D_2$, $^3H_6$) (process 1 in Fig. 5) and ($^3P_0$, $^3H_4$) → ($^1G_4$, $^1G_4$) (process 2). Eventually, from $^1D_2$ and $^1G_4$ other bilinear processes can populate even lower lying levels, such as ($^1D_2$, $^3H_4$) → ($^1G_4$, $^3F_3$) (process 3), and ($^1G_4$, $^3H_4$) → ($^3F_2$, $^3H_6$) (process 4). For this reason, we might expect to observe various emission bands throughout the NIR and MIR regions. The observed emission spectra are shown in Fig. 6(a)–6(d) with a possible transition assignment. Figure 6a shows a strong emission in the deep red region (650 nm, corresponding to 15400 $cm^{-1}$) that perfectly matches the $^3P_0 \rightarrow {}^3H_6$, $^3F_2$ transition and another much weaker emission band at around 750 nm (13300 $cm^{-1}$) whose assignment is clearly $^3P_0 \rightarrow {}^3F_3$. More uncertain is the assignment of the infrared emission shown in Fig. 6(b)

Optical Materials EXPRESS

at 950 nm (10500 $cm^{-1}$), 1.1 µm (9000 $cm^{-1}$), 1.6 µm (6000 $cm^{-1}$), and 1.8 µm (5500 $cm^{-1}$). Since $Pr^{3+}$ has a series of closely spaced levels with emission in the infrared, several energy level matchings are possible for these transitions. For example the peak at 10500 $cm^{-1}$ can be assigned to the $^1D_2 \rightarrow {}^3F_2$ or $^1G_4 \rightarrow {}^3H_4$ transition. The band at around 9000 $cm^{-1}$ could be composed by two different bands, but both regions match the $^1D_2 \rightarrow {}^3F_4$ and $^1G_4 \rightarrow {}^3H_4$ transition. Moreover, the band at around 6000 $cm^{-1}$ could be assigned to the $^1D_2 \rightarrow {}^1G_4$, $^1G_4 \rightarrow {}^3H_6$, and $^3F_3 \rightarrow {}^3H_4$ transition and that at around $5500^{-1}$ could be assigned both to the $^3F_2 \rightarrow {}^3H_4$ and $^1G_4 \rightarrow {}^3H_6$ transition. In order to have a more precise transition assignment we acquired emission spectra as a function of the incident power. The peak intensity was then linearly fitted in log-log scale to extract the pump-power dependence of the emission. Results are presented in Table 3. In many cases, the emission shows a super-linear dependence compatible with a two-photon process, and this confirms that the main energy transfer mechanism that populates the lower lying multiplets is cross-relaxation, instead of linear decay. As for the band at around 9000 $cm^{-1}$, peaks at energies higher and lower than 9000 $cm^{-1}$ have been analyzed separately and results show a very different behavior with the lower-energy band at around 8900 $cm^{-1}$ having a slope of 1.8, while the higher-energy part at around 9300 $cm^{-1}$ shows a slope of only 1.1. More careful inspection of Tab. 3 shows that three peaks show a nearly-quadratic dependence of the emission intensity (slopes between 1.7 and 1.9), and three other peaks show much lower slopes in the range between 1.1 and 1.4. Among the various possible assignments, the three bands with slopes between 1.5 and 2 have been assigned to transitions starting from the higher levels ($^3P_0$ and $^1D_2$), and those with slopes below 1.5 have been assigned to transitions from lower levels ($^1G_4$ and $^3F_{3,2}$). The result of this assignment is shown in Fig. 6(b) with only the band at around 5500 $cm^{-1}$ still remaining uncertain.

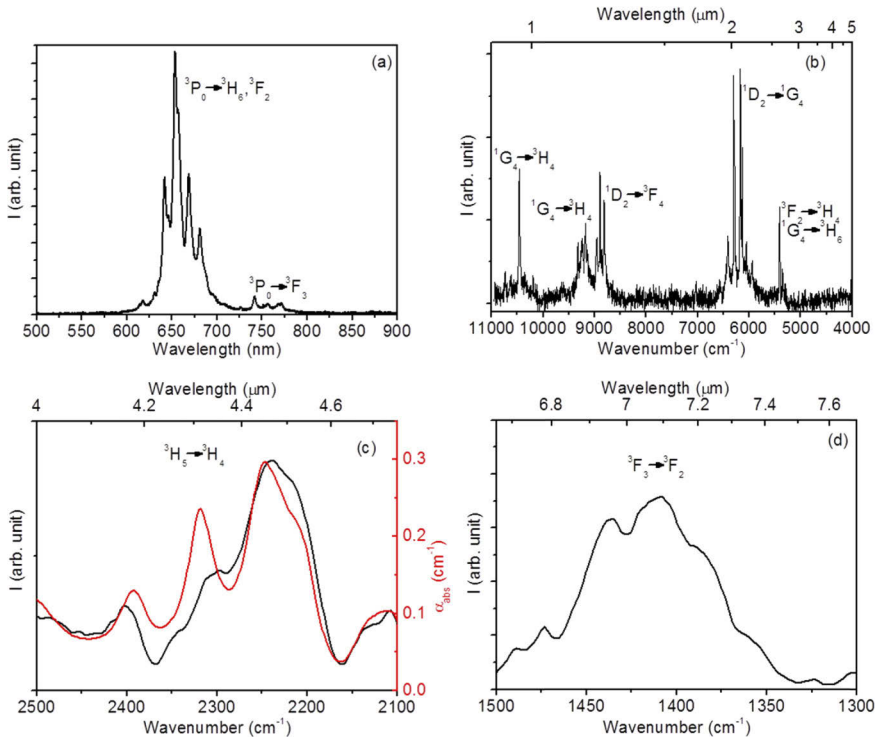


**Fig. 6.** a-d) Visible, NIR and MIR emissions of Pr:$Lu_2O_3$ under 450 nm excitation together with a possible transition assignment. The red line in (c) shows the ground state absorption into the $^3H_5$ multiplet.

Optical Materials EXPRESS

**Table 3. Slope fit of emission transitions**

| Transition energy ($cm^{-1}$) | Slope fit |
|---|---|
| 15300 | 1.7 |
| 13300 | Too weak to measure |
| 10500 | 1.4 |
| 9300 | 1.1 |
| 8900 | 1.8 |
| 6200 | 1.9 |
| 5400 | 1.2 |

Two other emission bands are observed at even longer wavelengths in the deep MIR, namely at 4.4 μm (2300 $cm^{-1}$, Fig. 6c) and 7 μm (1400 $cm^{-1}$, Fig. 6(d)). The emission at 4.4 μm can be assigned to the transitions $^3F_{3,4}\rightarrow{}^3H_6$, $^3H_6\rightarrow{}^3H_5$, or $^3H_5\rightarrow{}^3H_4$. Given the energy level scheme of $Pr^{3+}$, it is unlikely that $^3F_4$ experiences radiative emission because the energy gap to the lower lying level can be bridged with just 1 or 2 phonons of maximum energy in this crystal. Moreover, a comparison of the 4.4 μm emission with the $^3H_4\rightarrow{}^3H_5$ absorption data shows an almost perfect match, as reported in Fig. 6(c). Therefore, we propose to assign the 4.4 μm emission to the transition $^3H_5\rightarrow{}^3H_4$. The emission band at around 7 μm could be ascribed to $^3H_5\rightarrow{}^3H_4$, $^3H_6\rightarrow{}^3H_5$ or $^3F_3\rightarrow{}^3F_2$ but the best matching is with $^3F_3\rightarrow{}^3F_2$. Moreover, as the corresponding absorption spectra do not show lines in this region, we can also rule out $^3H_5\rightarrow{}^3H_4$. As a result, we propose to assign this band to the $^3F_3\rightarrow{}^3F_2$ transition.

These MIR emissions are weak, but we have to consider that our pumping scheme is not efficient for MIR emission. In fact, the diode emission at 450 nm populates the multiplet $^3P_2$ which is very far in energy from these low-lying levels. Other pumping schemes, e.g. pumping with a 1.5 μm Er-fiber laser, could lead to more efficient MIR emission. Moreover, it is remarkable that the emission bands at 4.4 μm and 7 μm are detected even if they correspond to less than 4 and 3 times the maximum host phonon energy, respectively.

## 4. Conclusions

In conclusion, we have reported absorption and emission spectra of $Pr^{3+}$:$Lu_2O_3$ in the MIR region from 1 to 10 μm. From absorption measurements, we directly observed the transparency cutoff at long wavelength that is around 8 μm, and we could identify absorption from the first five multiplets. In particular, we were able to observe direct absorption to $^3H_5$ that is located between 2200 $cm^{-1}$ and 3100 $cm^{-1}$. To the best of our knowledge, this multiplet has been directly observed for the first time. Low temperature measurements allowed us to extract the Stark sublevel positions of all these five multiplets and we revised the classical Dieke diagram for $Pr^{3+}$ in this compound. Moreover, we observed infrared emission of this material under visible diode laser pumping. We were able to observe several emission bands from 600 nm to beyond 7 μm. The pump power dependence of the corresponding emission intensities proved the main energy transfer mechanisms that populate the lower lying levels to be cross-relaxation processes and permitted us to assign the various bands to specific transitions. In particular, we observed for the first time MIR emission at 4.4 μm and 7 μm. The energy of the longest wavelength photons corresponds to an emission energy below three times the maximum phonon energy in this crystal host.

## Funding

Università di Pisa (PRA_2018_34); Bundesministerium für Bildung und Forschung (FKZ 13N13050); Bundesministerium für Bildung und Forschung (FKZ 13N14192).

Optical Materials EXPRESS

## Acknowledgments

A.To. acknowledges the support from the project PRA_2018_34 ("ANISE") from the University of Pisa. The research in Hamburg was funded within the projects "TSUNAMI" (BMBF, FKZ 13N13050) and supported by the excellence cluster "The Hamburg Centre for Ultrafast Imaging – Structure, Dynamics, and Control of Matter at the Atomic Scale" of the Deutsche Forschungsgemeinschaft. The IKZ was funded within the project "EQuiLa" (BMBF, FKZ 13N14192).

## References

1. S. R. Bowman, L. B. Shaw, B. J. Feldman, and J. Ganem, "Praseodymium solid state lasers at 5.2 and 7.2 microns-longest rare earth wavelengths to date," *in LEOS '95. IEEE Lasers and Electro-Optics Society 1995 8th Annual Meeting, Conference Proceedings*.
2. S. D. Jackson, "Towards high-power mid-infrared emission from a fibre laser," Nat. Photonics **6**(7), 423–431 (2012).
3. A. G. Okhrimchuk, L. N. Butvina, E. M. Dianov, I. A. Shestakova, N. V. Lichkova, V. N. Zagorodnev, and A. V. Shestakov, "Optical spectroscopy of the $RbPb_2Cl_5$:$Dy^{3+}$ laser crystal and oscillation at 5.5 μm at room temperature," J. Opt. Soc. Am. B **24**(10), 2690–2695 (2007).
4. M. R. Majewski, R. I. Woodward, J.-Y. Carree, S. Poulain, M. Poulain, and S. D. Jackson, "Emission beyond 4 μm and mid-infrared lasing in a dysprosium-doped indium fluoride ($InF_3$) fiber," Opt. Lett. **43**(8), 1926–1929 (2018).
5. B. M. Walsh, H. R. Lee, and N. P. Barnes, "Mid infrared lasers for remote sensing applications," J. Lumin. **169**, 400–405 (2016).
6. J.-L. Doualan and R. Moncorge, "Laser crystals with low phonon frequencies," Ann. Chim. (Cachan, Fr.) **28**(6), 5–20 (2003).
7. A. Ferrier, M. Velazquez, J.-L. Doualan, and R. Moncorge, "Spectroscopic investigation and mid-infrared luminescence properties of the $Pr^{3+}$-doped low phonon single crystals $CsCdBr_3$, $KPb_2Cl_5$ and $Tl_3PbBr$," J. Lumin. **129**(12), 1905–1907 (2009).
8. M. Fibrich, J. Šulc, R. Král, V. Jarý, M. Němec, H. Jelínková, A. Bystřický, P. Zemenová, and M. Nikl, "Luminescence study of rare-earth (RE)-doped low-energy phonon $RbPb_2Cl_5$ crystals for mid-infrared (IR) lasers emitting above 4.5 μm wavelength," Laser Phys. **29**(7), 075801 (2019).
9. B. Denker and E. Shklovsky (eds.) "Handbook of Solid-State Lasers: Materials, Systems and Applications," Woodhead Publishing Series in Electronic and Optical Materials (2013) ISBN: 9780857092724.
10. P. A. Loiko, K. V. Yumashev, R. Schödel, M. Peltz, C. Liebald, X. Mateos, B. Deppe, and C. Kränkel, "Thermo-optic properties of Yb:$Lu_2O_3$ single crystals," Appl. Phys. B: Lasers Opt. **120**(4), 601–607 (2015).
11. C. Krankel, "Rare-Earth-Doped Sesquioxides for Diode-Pumped High-Power Lasers in the 1-, 2-, and 3-μm Spectral Range," IEEE J. Sel. Top. Quantum Electron. **21**(1), 250–262 (2015).
12. A. Heuer, C. J. Saraceno, K. Beil, G. Huber, and C. Kränkel, "Efficient OPSL-pumped mode-locked Yb:$Lu_2O_3$ laser with 67% optical-to-optical efficiency," Sci. Rep. **6**(1), 19090 (2016).
13. D. Kulesza, P. Bolek, A. J. J. Bos, and E. Zych, "$Lu_2O_3$-based storage phosphors. An (in)harmonious family," Coord. Chem. Rev. **325**, 29–40 (2016).
14. A. M. Heuer, P. von Brunn, G. Huber, and C. Kränkel, "$Dy_{3+}$:$Lu_2O_3$ as a novel crystalline oxide for mid-infrared laser applications," Opt. Mater. Express **8**(11), 3447–3455 (2018).
15. L. Pauling and M. Shappell, "The Crystal Structure of Bixbyite and the C-Modification of the Sesquioxides," Z. Kristallogr. - Cryst. Mater. **75**(1), 128–142 (1930).
16. M. Guzik, J. Pejchal, A. Yoshikawa, A. Ito, T. Goto, M. Siczek, T. Lis, and G. Boulon, "Structural Investigations of $Lu_2O_3$ as Single Crystal and Polycrystalline Transparent Ceramic," Cryst. Growth Des. **14**(7), 3327–3334 (2014).
17. R. Peters, C. Kränkel, K. Petermann, and G. Huber, "Crystal growth by the heat exchanger method, spectroscopic characterization, and laser operation of high purity $Yb^{3+}$-doped $Lu_2O_3$," J. Cryst. Growth **310**(7-9), 1934–1938 (2008).
18. A. Kaminskii, "Laser Crystals: Their Physics and Properties," (Springer Berlin Heidelberg, 2013).
19. G. H. Dieke and H. M. Crosswhite, "The Spectra of the Doubly and Triply Ionized Rare Earths," Appl. Opt. **2**(7), 675 (1963).
20. J. L. Pascual, Z. Barandiaran, and L. Seijo, "Ab initio theoretical study of luminescence properties of $Pr^{3+}$-doped $Lu_2O_3$," Theor. Chem. Acc. **129**(3-5), 545–554 (2011).
21. V. Peters, "Growth and Spectroscopy of Ytterbium-doped Sesquioxides (Berichte aus der Physik)," Shaker Verlag GmbH, Germany (29 October 2001) ISBN-10: 3826594797
22. R. P. Leavitt, J. B. Gruber, N. C. Chang, and C. A. Morrison, "Optical spectra, energy levels, and crystal-field analysis of tripositive rare-earth ions in $Y_2O_3$. II. Non-Kramers ions in $C_2$ sites," J. Chem. Phys. **76**(10), 4775–4788 (1982).
23. V. Peters, "Spektroskopie und Lasereigenschaften erbium- und praseodymdotierter hochschmelzender Oxide," Diploma Thesis, Hamburg University (1998).
24. D. Bloor and J. R. Dean, "Spectroscopy of rare earth oxide systems: I. Far infrared spectra of the rare earth sesquioxides, cerium dioxide, and nonstoichiometric praseodymium and terbium oxides," J. Phys. C: Solid State Phys. **5**(11), 1237–1252 (1972).
25. N. T. McDewitt and A. D. Davison, "Infrared Lattice Spectra of Cubic Rare Earth Oxides in the Region 700 to 50 $cm^{-1}$," J. Opt. Soc. Am. **56**(5), 636–638 (1966).